The Astrophysical Journal, 977:122 (8pp), 2024 December 10 https://doi.org/10.3847/1538-4357/ad9023

Challenges for Fast Radio Bursts as Multimessenger Sources from Binary Neutron Star Mergers

Mohit Bhardwaj[1], Antonella Palmese[1], Ignacio Magaña Hernandez[1,2], Virginia D'Emilio[3], and Soichiro Morisaki[4]
[1] McWilliams Center for Cosmology, Department of Physics, Carnegie Mellon University, Pittsburgh, PA 15213, USA; mohitb@andrew.cmu.edu
[2] University of Wisconsin-Milwaukee, Milwaukee, WI 53201, USA
[3] Cardiff University, Cardiff CF24 3AA, UK
[4] Institute for Cosmic Ray Research, The University of Tokyo, 5-1-5 Kashiwanoha, Kashiwa, Chiba 277-8582, Japan
Received 2024 September 30; revised 2024 October 31; accepted 2024 October 31; published 2024 December 9

Abstract

Fast radio bursts (FRBs) are millisecond-duration transients from extragalactic sources, with their origins remaining a topic of active debate. Among the proposed progenitors, binary neutron star (BNS) mergers are compelling candidates for some nonrepeating FRBs. However, associating FRBs with BNS mergers cannot be based solely on low chance coincidence probability. This study delineates necessary criteria for associating FRBs with BNS mergers, focusing on the postmerger ejecta environment. To underscore the significance of these criteria, we scrutinise the proposed association between GW190425 and FRB 20190425A, considering the requirement for the FRB signal to traverse the dense merger ejecta without significant attenuation to remain detectable at 400 MHz. Our investigation reveals that if the FRB is linked to the gravitational-wave (GW) event, the GW data support a highly off-axis configuration, with a probability of the BNS merger viewing angle $p(\theta_v > 30^\circ)$ being $\approx$99.99%. This strongly excludes an on-axis system, which is required for this FRB to be detectable. We also find faraway FRB emission models inadequate to explain the FRB 20190425A–GW190425 connection. Thus, we conclude that GW190425 is not related to FRB 20190425A. We discuss the implications for future multimessenger observations, suggesting that BNS merger remnants are unlikely to account for more than 1% of FRB sources. This finding implies that short gamma-ray bursts, which are expected to occur in only a fraction of all BNS mergers, cannot account for the overall characteristics of the FRB host population.

Unified Astronomy Thesaurus concepts: Radio transient sources (2008); Radio pulsars (1353)

1. Introduction

Fast radio bursts (FRBs) are intense flashes of highly coherent radio waves (brightness temperature $\sim 10^{36}$ K) that exhibit duration ranging from microseconds to milliseconds (D. R. Lorimer et al. 2007). These bursts can be detected across vast extragalactic distances, making them a promising cosmological probe (J. M. Cordes & S. Chatterjee 2019; M. Caleb & E. Keane 2021; E. Petroff et al. 2022). Since the discovery of the first FRB in 2007, over 1000 FRBs have been reported to date.[5] Nevertheless, their origins remain a topic of continued scientific investigation and speculation. Recent years have seen significant advancements in understanding the underlying source population of these cosmic events. For example, CHIME/FRB Collaboration et al. (2021) inferred a sky rate of bright FRBs (bursts of fluence $\geqslant 5$ Jy ms at 600 MHz) to be $\sim$600 FRBs/sky/day and estimated the volumetric rate of FRBs with a fiducial energy of $\sim 10^{39}$ erg to be $\sim 10^5$ FRBs/yr/Gpc^3 (K. Shin et al. 2023). Moreover, there exists a substantial subpopulation of FRBs that repeats (L. G. Spitler et al. 2016; CHIME/FRB Collaboration et al. 2019a, 2019b; E. Fonseca et al. 2020; M. Bhardwaj et al. 2021a; P. Kumar et al. 2021; A. E. Lanman et al. 2022; R. McKinven & CHIME/FRB Collaboration 2022; C. H. Niu et al. 2022; B. C. Andersen et al. 2023). These observations suggest that most of the FRBs, particularly those in the local Universe, have noncataclysmic origins (M. Bhardwaj et al. 2021b) and are likely have progenitors formed via core-collapse supernovae (M. Bhardwaj et al. 2024). However, cataclysmic origins for a subset of FRBs that do not exhibit repetition cannot be ruled out.

Several FRB models propose cataclysmic events, such as the merger of compact binary systems with neutron stars and/or black holes, to explain a fraction of nonrepeating FRBs (T. Totani 2013; H. Falcke & L. Rezzolla 2014; C. M. F. Mingarelli et al. 2015; J.-S. Wang et al. 2016; B. Zhang 2016; M. A. Abramowicz et al. 2018). It is worth noting that many of these events in the local Universe ($\sim$100 Mpc) can be detected using current-generation gravitational-wave (GW) detectors (R. Abbott et al. 2021; The LIGO Scientific Collaboration et al. 2023). Binary neutron star (BNS) mergers, within the realm of cataclysmic events, are regarded as potential sources of FRB-like signals at different stages of the merger: prior to, during, or after the merger (for the full list of models, see K. Gourdji et al. 2020). Recently, A. Moroianu et al. (2023) reported a possible association, at the 2.8σ level, between GW190425 (B. P. Abbott et al. 2020b), the second BNS merger to be detected in GWs, and FRB 20190425A (CHIME/FRB Collaboration et al. 2021; M. Bhardwaj et al. 2024). GW190425 was detected by the LIGO–Virgo–KAGRA (LVK) GW detector network during the first half of their third observing run, O3a (R. Abbott et al. 2024). The immediately interesting aspect of this merger was that its chirp ($\sim 1.44\,M_\odot$) and total mass ($\sim 3.4\,M_\odot$) were significantly larger than any other known BNS system. Because the LIGO Hanford detector was offline for $\sim$2 hr around the GW event time, the sky localization of this event is not precise

[5] For a complete list of known FRBs, see the Transient Name Server (O. Yaron et al. 2020).

(90% credible localization region is 7461 deg^2). Moreover, since it was at a significantly larger distance (luminosity distance $d_L = 159^{+69}_{-71}$ Mpc) compared to GW170817 (∼40 Mpc), any associated electromagnetic counterpart would have been significantly fainter, and the large localization volume challenged both follow-up searches and high-confidence association for any candidate counterpart.

FRB 20190425A was discovered by the Canadian Hydrogen Intensity Mapping Experiment/Fast Radio Burst (CHIME/FRB; CHIME/FRB Collaboration et al. 2021) project ≈2.5 hr after the GW alert, and according to F. H. Panther et al. (2022), it most likely occurred in the host galaxy UGC 10667 (probability of true association ≈0.79). This association was found to be true by M. Bhardwaj et al. (2024) using CHIME/FRB baseband localization (chance association probability $< 0.1\%$). Given the total mass of GW170817 was determined to be $3.4^{+0.3}_{-0.1}\,M_\odot$, the LVK collaboration suggested that the merger likely resulted in the prompt collapse of the two neutron stars into a black hole, based on current constraints on the equation of state (EOS) for dense nuclear matter (B. Abbott et al. 2020). However, to address the discrepancy between this interpretation and the 2.5 hr postmerger delay, A. Moroianu et al. (2023) and B. Zhang (2023) proposed a scenario where the merger led to the formation of a highly spinning supramassive neutron star (SMNS) with an extremely strong magnetic field ($\geqslant 10^{14}$ Gauss) and an EOS consistent with quark models. This raises two key questions: Can FRBs be expected from such a system? And how can empirical evidence be used to either support or refute these potential associations?

In this work, we present the necessary conditions based on astrophysical and GW constraints that any plausible FRB and BNS merger association must satisfy before even considering the probability of a chance coincidence between the two events. This is crucial because the FRB signal must traverse the high-density merger ejecta without experiencing significant attenuation to be detectable at ∼1 GHz. To demonstrate the use of the aforementioned constraint, we reconsider the association between GW190425 and FRB 20190425A using two classes of constraints that were not discussed in A. Moroianu et al. (2023): (1) an updated GW parameter estimation under the assumption that UGC 10667 is the host galaxy of both FRB 20190425A and GW190425, which is discussed in Section 2, and (2) the effect of the BNS merger ejecta in the propagation of the FRB signal, which is discussed in Section 3. Considering these new constraints, we examine the association by evaluating the consistency of the measured viewing angle with the blitzar model invoked in A. Moroianu et al. (2023). Furthermore, we determine the maximum ejecta mass required to enable the propagation of the FRB signal at 400 MHz without experiencing any noticeable attenuation. Both of these constraints independently disfavor the proposed association of GW190425 and FRB 20190425A as presented in 4.1. Moreover, we also investigate the prospects of "faraway" FRB emission models to explain the association in Section 4.2 and conclude that these models too face severe challenges in explaining the association. Finally, we discuss the implications of our findings for future associations between FRBs and BNS merger remnants in Section 4.3 and conclude in Section 5. In all the analyses presented in this work, we assume the Planck 2015 cosmological model (Planck Collaboration et al. 2015).

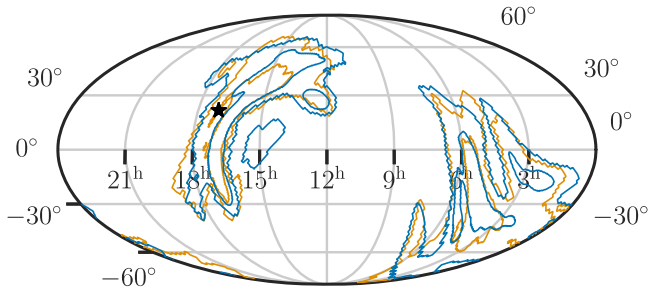

Figure 1. Sky localization regions using both the low-spin (blue) and high-spin (yellow) posterior samples as reported in B. Abbott et al. (2020). We show both the 50% and 90% confidence intervals for each case and show the location of UGC 10667.

2. Parameter Estimation with UGC 10667 as the Host Galaxy

In order to assess the viability of UGC 10667 as the host for GW190425 and FRB 20190425A, we employ the framework described in I. Magaña Hernandez et al. (2024) to estimate the inclination angle (i) posterior given that GW190425 is linked with FRB 20190425A, which is now robustly associated with UGC 10667. Here, we present a succinct overview of the Bayesian parameter estimation procedure employed in this study. For more detail, refer to I. Magaña Hernandez et al. (2024). We use the `BILBY` library (G. Ashton et al. 2019; I. M. Romero-Shaw et al. 2020) and the `DYNESTY` nested sampler package (J. S. Speagle 2020). The waveform model used in the analysis is `IMRPhenomPv2_NRTidal` (T. Dietrich et al. 2017, 2019), which includes both precession and tidal effects. To make the analysis computationally inexpensive, we use the reduced-order quadrature technique (R. Smith et al. 2016; A. Baylor et al. 2019).

Following the LVK analysis conventions presented in R. Abbott et al. (2024), we perform two sets of analyses with different spin priors, namely, a low-spin and a high-spin prior where we assume uniform distributions on the dimensionless spin magnitudes for both components to be within the ranges $\chi < 0.05$ and $\chi < 0.89$, respectively. The prior probability distributions on the remaining binary parameters used in this work are the same as those used in R. Abbott et al. (2024), except that (1) we fix the sky position, i.e., we set the sky location to the location of UGC 10667 $(\alpha,\ \delta) = (255.^\circ72,\ 21.^\circ52)$ from R. Ahumada et al. (2020), and (2) we additionally fix the redshift to that of UGC 10667 (spectroscopic redshift, $z = 0.03136 \pm 0.00009$; K. N. Abazajian et al. 2009). It is worth noting that changing the position of the BNS merger within the 90% confidence baseband localization region of the FRB estimated by M. Bhardwaj et al. (2024) does not have any meaningful impact on our results. Finally, for completeness, we show the sky localization posteriors and the location of UGC 10667 in Figure 1. We note that the location of the galaxy is within the 90% confidence region under both low- and high-spin assumptions.

We then calculate the viewing angle, $\theta_v = \min(\theta_{\rm JN}, 180^\circ - \theta_{\rm JN})$, using the measured inclination angles $\theta_{\rm JN}$ for each of the cases considered. In particular, we note that we can measure the viewing angle to GW190425 under the fixed position assumption since the measured redshift to UGC 10667 breaks the distance-inclination degeneracy (B. F. Schutz 2011). We report our viewing angle measurements in Table 1 using the low-spin and high-spin prior results with both the fixed sky and fixed position assumptions.

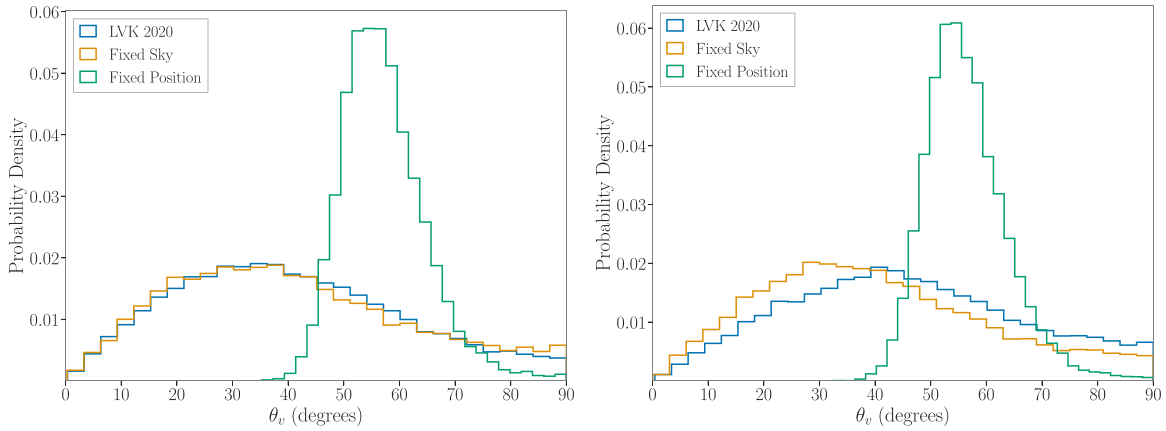

Figure 2. Posterior distributions on the viewing angle θ_v for GW190425 for both the low-spin (left panel) and high-spin (right panel) priors under the fixed sky location and fixed position assumptions as described in Section 2. For both cases, we also show the viewing angle posteriors computed using the results of B. Abbott et al. (2020) for reference.

Table 1
Summary of the Estimated Viewing Angle for GW190425 Using Both the Low-spin and High-spin Priors under the Fixed Sky and Fixed Position Assumptions as Described in Section 2

	Low Spin Prior		High Spin Prior	
	Fixed Sky	Fixed Position	Fixed Sky	Fixed Position
Viewing angle θ_v	$37.8^{+42.4}_{-27.5}$ deg	$56.1^{+14.3}_{-9.7}$ deg	$37.8^{+41.3}_{-26.9}$ deg	$55.6^{+14.3}_{-9.2}$ deg

From this analysis, we infer that our inclination angle constraints are agnostic to the assumed spin of the merger (also see I. Magaña Hernandez et al. 2024). Additionally, we show the marginalized posteriors on θ_v for the low- and high-spin prior cases in Figure 2.

3. Characterizing Propagation Effects on 400 MHz FRB Emission

In A. Moroianu et al. (2023), the authors employed the "blitzar" mechanism first proposed by H. Falcke & L. Rezzolla (2014) to provide an explanation for FRB 20190425A at time $t_{\rm FRB} = 2.5$ hr after the GW190425 event. In doing so, the authors made two assumptions: first, that GW190425 represents a BNS merger event, and second, that the resulting postmerger remnant is an SMNS. We note that the validity of both assumptions is still being strongly debated (B. P. Abbott et al. 2020a; R. Essick & P. Landry 2020; R. J. Foley et al. 2020; M.-Z. Han et al. 2020; C. Barbieri et al. 2021). In the blitzar mechanism, when a highly magnetized SMNS collapses to form a black hole, it ejects its magnetosphere as the magnetic fields cannot puncture the event horizon, as dictated by the no-hair theorem (N. Gürlebeck 2015). This generates strong magnetic shock waves that accelerate electron and positron pairs already present in the magnetosphere to relativistic velocities. The FRB is produced via curvature radiation emission when these relativistic particles follow the distorted ejected magnetic field lines over spatial scales $\approx c\Delta t$, where Δt is the temporal width of the FRB. However, we note that is it still unclear if the curvature radiation can be operational in such a chaotic scenario (P. Kumar et al. 2017). We ignore these concerns in the following discussions and assess the feasibility of this scenario for this specific GW event.

In order to estimate the ejecta electron number density, $n_{\rm ej}$, we assume spherically symmetric and homogeneous ejecta of mass $M_{\rm ej}$, which expands with an average velocity $v_{\rm ej} = 0.4c$, where c is the speed of light and has the electron fraction $Y_e = 0.2\, Y_{e,0.2}$, as per the results from the numerical relativity study by D. Radice et al. (2018). The ejecta is fully ionized[6] and composed of heavy elements with $Z/A \approx 2$. Our choice of these fiducial values is informed by both recent simulation results and observations from GW170817 (K. Hotokezaka et al. 2013; A. Perego et al. 2017; M. W. Coughlin et al. 2018). Note that the spherical symmetry of the early epoch ejecta appears reasonable for various analytical estimates (B. D. Metzger 2019) and has been recently argued to be true for AT2017gfo, the kilonova associated with the GW170817 event (A. Sneppen et al. 2023). In Section 4.1, we discuss the impact of a nonspherical ejecta on our results.

In the spherically symmetric ejecta scenario, we estimate $n_{\rm ej}$ to be

$$n_{\rm ej} \approx \frac{3M_{\rm ej}Y_e}{8\pi m_p (v_{\rm ej}t)^3} = 1.8 \times 10^{14} \frac{M_{\rm ej}}{M_\odot} Y_{e,0.2} v_{\rm ej,0.4c}\ {\rm cm}^{-3}, \quad (1)$$

where m_p is the proton mass. Note that in all of our calculations, we fix $t = t_{\rm FRB} = 2.5$ hr.

In order for us to observe FRB 20190425A, which exhibits a flat and broadband frequency spectrum (the FRB is detected in the full CHIME band, i.e., 400–800 MHz; CHIME/FRB Collaboration et al. 2021), the ambient environment must be sufficiently rarefied and, hence, should be optically thin to various propagation effects that can suppress the FRB signal at 400 MHz. Using this constraint, we now derive an upper limit on the ejecta mass of GW190425 for different propagation effects described below.

[6] For GW190425, this assumption is challenged by D. Radice et al. (2024) based on their numerical relativity simulation results. However, this will not affect the major conclusion from this study.

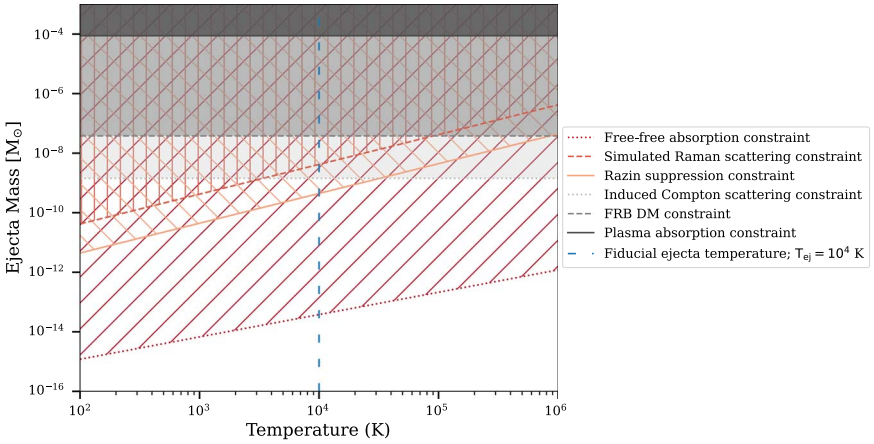

Figure 3. Derived constraints on the BNS ejecta mass ($M_{\rm ej}$) if FRB 20190425A is indeed associated with GW190425. Hatched regions are excluded using ejecta temperature ($T_{\rm ej}$)–dependent propagation effects, and shaded regions are excluded due to constraints that are independent of the ejecta temperature, as discussed in Section 3.

3.1. Plasma Absorption Constraint

The plasma frequency ν_p of electrons in the BNS ejecta must be smaller than 400 MHz; otherwise, the FRB signal would have been absorbed. Therefore, ν_p is given by

$$\nu_p = \frac{1}{2\pi}\sqrt{\frac{n_{\rm ej}e^2}{m_e\varepsilon_0}} < 400\ \text{MHz}, \tag{2}$$

where m_e is the electron mass, ε_0 is the permittivity of free space, and e is the electron charge. Using Equation (1) in Equation (2), we get $M_{\rm ej} < 8\times10^{-5}M_\odot$.

3.2. FRB Dispersion Measure Constraint

CHIME/FRB Collaboration et al. (2021) reported the dispersion measure (DM) of FRB 20190425A, defined as

$$\text{DM} = \int_0^L n_e\, dx, \tag{3}$$

where n_e is the free electron number density and L is the comoving distance of the FRB source from us, to be 128.1 pc cm^{-3}. Note that there are several astrophysical components that contribute to the FRB DM, namely, the Milky Way interstellar medium (MW ISM) and its halo, the intergalactic medium (IGM), and the FRB host and its local environment (in this case, the local environment would be the BNS ejecta), such that $\text{DM}_{\rm FRB} = \text{DM}_{\rm MWISM} + \text{DM}_{\rm MWhalo} + \text{DM}_{\rm IGM} + \text{DM}_{\rm host} + \text{DM}_{\rm BNSejecta} = 128.1$ pc cm^{-3}. Here, $\text{DM}_{\rm IGM} \sim 30$ pc cm^{-3} using the Macquart relation (J.-P. Macquart et al. 2020), if we assume UGC 10667 at redshift = 0.03136 as the FRB host, $\text{DM}_{\rm MW\ ISM} \sim 40$ pc cm^{-3} along the FRB line-of-sight using the NE2001 (J. M. Cordes & T. J. W. Lazio 2002) and YMW16 (J. M. Yao et al. 2017) Galactic electron density distribution models, and $\text{DM}_{\rm MW\ halo} \sim 30$ pc cm^{-3} from the S. Yamasaki & T. Totani (2020) Milky Way halo model. Using these values, we estimate $\text{DM}_{\rm host} + \text{DM}_{\rm BNSejecta} \sim 30$ pc cm^{-3} and compute an upper limit on the ejecta mass assuming $\text{DM}_{\rm host} = 0$ pc cm^{-3} using Equations (1) and (3) to be $\lesssim 4\times10^{-8}\,M_\odot$. Note that uncertainties in the DM estimates of different astrophysical components would result in <1 dex error in our upper-limit estimate.

3.3. Induced Compton Scattering Constraint

Induced Compton scattering, also known as stimulated Compton scattering, is a process in which a photon collides with a free-charged particle, such as an electron, and transfers a portion of its energy to the particle (D. B. Wilson 1982). As a result of the collision, the photon is scattered and its energy is reduced, while the electron gains kinetic energy. In the case of short (duration $= \Delta t \sim 1$ ms) coherent radio emission, like FRB, with brightness temperature $T_{\rm B} \sim 10^{36}$ K traversing a nonrelativistic plasma, the induced Compton scattering optical depth can be estimated using Equations (6) and (14) from Y. Lyubarsky (2008):

$$\tau_C = \frac{3\sigma_T c k_{\rm B}}{8\pi m_{\rm e}} n_{\rm ej} T_{\rm B} \frac{\Delta t^3}{v_{\rm ej} t^2} < 1, \tag{4}$$

where $\sigma_{\rm T}$ is the Thomson cross section of electrons and $k_{\rm B}$ is the Bolzmann constant. Equation (4) gives $M_{\rm ej} \lesssim 2\times10^{-9}\,M_\odot$.

3.4. Simulated Raman Scattering Constraint

In the case of highly coherent sources, like FRBs, the energy density of the radio waves is so high that it can create Langmuir waves in dense ejecta plasma through a process called parametric decay instability (A. Levinson & R. Blandford 1995). The Langmuir waves can then interact with FRB emission and induce Raman scattering, in which the photons are scattered away and the FRB signal decays away to a lower frequency and momentum state. The effect of simulated Raman scattering is significant in our case when

$$400 \gtrsim 130\left(\frac{n_{\rm e}}{\text{cm}^{-3}}\right)^{1/2}\left(\frac{T_{\rm ej}}{\text{K}}\right)^{-1/2}\text{MHz}. \tag{5}$$

Figure 3 shows the maximum BNS ejecta mass as a function of the ejecta temperature. At the fiducial ejecta temperature $T_{\rm ej}$ of kilonova emission of $\approx 10^4$ K (B. D. Metzger 2019), we estimate $M_{\rm ej} \lesssim 4\times10^{-9}\,M_\odot$.

3.5. Razin Suppression Constraint

The Razin suppression (V. Razin 1960), also known as the Razin–Tsytovich effect (D. B. Melrose 1972), is a nonlinear plasma effect in the presence of a strong magnetic field that can result in the attenuation of radio emission at $\nu \gtrsim \nu_p$. In our case,

it can suppress the production of bunched coherent curvature emission (J. Arons & J. J. Barnard 1986) at a frequency below the Razin cutoff frequency ($\nu_{\rm R}$). We use the following relation from V. Ravi & A. Loeb (2019):

$$\nu_{\rm R} = 400\left(\frac{n_e}{n_{\rm ej}}\right)^{1/2}\left(\frac{T_{\rm ej}}{10^4\ {\rm K}}\right)^{-1/2} < 400\ {\rm MHz}, \quad (6)$$

where n_e is the number density of thermal plasma, and estimate $M_{\rm ej} \lesssim 5 \times 10^{-10}\,M_\odot$ at $T_{\rm ej} = 10^4$ K. At other temperatures, the maximum $M_{\rm ej}$ constraint is shown in Figure 3.

3.6. Free–Free Absorption Constraint

An FRB signal can interact with the free ions and electrons in the surrounding ejecta medium through free–free absorption, which shows a characteristic frequency dependence $\sim\nu^{-2}$ when the free–free optical depth ($\tau_{\rm ff}$) > 1. Note that the amount of absorption of the FRB signal depends on both the electron number density and temperature ($T_{\rm ej}$) of the ejecta. In our case, as the FRB spectrum does not exhibit such behavior, $\tau_{\rm ff}$ must be < 1 at 400 MHz. At $T_{\rm ej} \approx 10^4$ K, we estimate an upper limit on $M_{\rm ej}$ at $\nu = 0.4$ GHz using Equation (35) from F. Y. Wang et al. (2020), i.e.,

$$\tau_{\rm ff} \simeq 2.3 \times 10^{28} Y_{\rm e,0.2}^2 v_{\rm ej,0.4c}^{-5} \nu_{0.4}^{-2} T_{\rm ej,4}^{-3/2} M_{\rm ej,\odot}^2, \quad (7)$$

to be $4 \times 10^{-14} M_\odot$. This is the most stringent constraint on the $M_{\rm ej}$. The $M_{\rm ej}$ estimates at other $T_{\rm ej}$ are shown in Figure 3. We note that changing other kilonova ejecta parameters within reasonable ranges will not affect this estimate by more than 1 order of magnitude, so the constraint remains very stringent.

3.7. Synchroton Self-absorption Constraint

If the postmerger remnant is an SMNS, it is expected to have a strong magnetic field of at least 10^{14} G (B. Giacomazzo et al. 2015), which could create a pulsar wind nebula after interacting with the ejecta. This nebula would accelerate charged particles to relativistic speeds and hinder the transmission of the FRB signal via synchrotron self-absorption. Hydrodynamic simulations by S. Yamasaki et al. (2018) suggest that the dynamical ejecta would obstruct the escape of coherent radio emission until ~1–10 yr after the merger. However, quantifying the effect of ejecta mass on the synchrotron self-absorption optical depth is a complex problem that depends on various parameters, such as the electron energy spectrum. Further discussion on this will be presented elsewhere.

4. Discussion

4.1. Are FRB 20190425A and GW190425 Related?

In Section 3, we showed that if the FRB is indeed associated with GW190425, then for the FRB emission to pass through the BNS ejecta without suffering significant attenuation due to different propagation effects, the ejecta mass has to be $\lesssim 10^{-14}\,M_\odot$. This is at least 12 orders of magnitude smaller than what has been observed in the case of GW170817 and predicted by numerical simulations ($\sim 10^{-2}$–$10^{-4}\,M_\odot$; K. Hotokezaka et al. 2013; T. Dietrich et al. 2015; D. Radice et al. 2016; B. P. Abbott et al. 2017; R. Dudi et al. 2022; A. Henkel et al. 2023).

The only possible scenario in which the FRB emission can escape through the BNS ejecta is if the outflow electron number density is extremely low (~0.1 cm^{-3} using $M_{\rm ej} < 10^{-14}\,M_\odot$ in Equation (1)). To explain this, B. Zhang (2014) proposed a scenario in which the FRB is emitted in the direction of the relativistic jet generated after the merger of BNS, which is observed as a short-duration gamma-ray burst (GRB), where the jet's action can lead to a substantial reduction in the surrounding ejecta density. In this case, we expect the inclination angle of the merger to be <30° (D. Radice et al. 2016; Z.-P. Jin et al. 2018; S. Biscoveanu et al. 2020; E. Burns 2020). However, as shown in Table 1 and Figure 3, if the FRB is associated with UGC 10667, we expect the BNS merger viewing angle to be $\theta_v \sim 60°$, making the GW event an off-axis merger. In fact, our posteriors do exclude an on-axis system and an off-axis system similar to GW170817 (J. Granot et al. 2018) at $p(\theta_v > 30°) = 99.99\%$. We note that this conclusion does not change whether we assume a low- or high-spin prior. This consideration also rules out a possible GW–FRB association with the weak GRB detection by the Anti-Coincidence Shield of the International Gamma-Ray Astrophysics Laboratory (A. S. Pozanenko et al. 2020), as opposed to the consistency with the GW–FRB association, reported in A. Moroianu et al. (2023). Finally, we note that it is not clear if the polar region remains low density after ~2.5 hr the launch of the relativistic jet (B. Margalit et al. 2019; B. D. Metzger 2019; A. Sneppen et al. 2023). More importantly, MHD simulations suggest that forming a relativistic jet when the BNS merger remnant is a neutron star is more challenging than when it is a black hole (R. Ciolfi & J. V. Kalinani 2020; H. Hamidani & K. Ioka 2021). One solution to this problem would be that a jet is launched during the collapse of an SMNS into a black hole, as hypothesized by M. Ruiz et al. (2016). However, the feasibility of this mechanism is yet to be explored.

We note that our electron density calculations rely on the assumption that the BNS ejecta is isotropic, whereas in reality, some degree of anisotropy is expected (e.g., S. Darbha & D. Kasen 2020). For instance, it is possible that the wind outflow from the magnetar remnant could create a cavity in the merger ejecta (N. Bucciantini et al. 2006). This is particularly feasible for the wind outflow to facilitate the evacuation of matter in the polar region (R. Bühler & M. Giomi 2016). However, the efficiency of these winds in significantly affecting the spatial distribution of ejecta matter is yet to be investigated (G.-L. Wu et al. 2022). More importantly, the wind outflow is expected to be roughly isotropic in the equatorial plane due to the toroidal configuration of the magnetic fields (N. Bucciantini et al. 2006), which is a likely more appropriate in our case. However, if the remnant resulting from the BNS merger is an SMNS, the substantial neutrino luminosity emitted by the remnant itself may contribute to the ejection of a significant mass ($\sim 10^{-3}$–$10^{-2}\,M_\odot$; L. Dessart et al. 2009; A. Perego et al. 2014; D. Martin et al. 2015). Additionally, it is expected that the SMNS would have a strong ordered magnetic field, as seen in cosmological simulations (C. Palenzuela et al. 2022), which can further enhance the outflow (T. A. Thompson et al. 2004; B. D. Metzger et al. 2018).

Moreover, in most general relativistic simulations of BNS mergers, the ejecta is found to be mostly distributed over a broad ~60° angle from the equatorial plane (D. Radice et al. 2016), with additional squeezed dynamical ejecta possible along the polar region (e.g., D. Kasen et al. 2017). This would not affect our conclusion because if the GW event were associated with the FRB, the inclination angle (see Figure 2) would still be within a region where significant ejecta is

expected. Note that our minimum M_{ej} constraint only considers dynamical ejecta, which is composed of a combination of tidally and shock-driven ejecta, and ignores the contribution from the accretion disk, which formed after the neutron star merger and is an important contributor to the total ejecta from the merger ($\gtrsim 10^{-4}\,M_{\odot}$; C. J. Krüger & F. Foucart 2020). For the highly off-axis BNSs, such as the one under discussion, it is likely that the FRB signal would also have to pass through this component of the ejecta, which would make our derived minimum M_{ej} constraint orders of magnitude more conservative. This further weakens the case for the FRB-GW association.

Finally, there are significant challenges associated with the assumption that the FRB-GW event results in a strongly magnetized millisecond SMNS. First, a kilonova with a magnetar central engine would be significantly brighter than one without such an engine (N. Sarin et al. 2022b). Therefore, if GW190425 is indeed associated with the host galaxy of FRB 20190425A, an optical counterpart should have been detected in follow-up observations, but no promising optical counterpart was found at the proposed FRB host location (G. Hosseinzadeh et al. 2019; M. W. Coughlin et al. 2019; S. Smartt et al. 2024). Second, the 2.5 hr delay between GW190425 and FRB 20190425A conflicts with theoretical and numerical predictions for SMNS collapse times. With a stiffer EOS, as invoked to explain the FRB-GW event (A. Moroianu et al. 2023), the collapse time to a black hole is expected to be significantly shorter, $\lesssim 10^3$ s (A. Li et al. 2016; N. Sarin et al. 2020), which is in tension with the observed 9000-second delay. Lastly, if the GW190425 remnant is indeed an SMNS, it would suggest that the remnant of GW170817 was a stable neutron star, a hypothesis that is widely debated in the literature (H. Gao et al. 2020, and reference therein).

In conclusion, all these arguments make the GW190425-FRB 20190425A association highly unlikely.

4.2. Are Faraway Models Compatible with FRB 20190425A and GW190425?

In Section 4.1, we discuss challenges associated with models where the FRB is produced within the magnetosphere of an SMNS, a scenario commonly invoked in post-merger FRB models (see A. Moroianu et al. 2023). However, if the FRB is generated farther from the magnetosphere ($\gtrsim 10^{13}$ cm) via the synchrotron maser mechanism (B. D. Metzger et al. 2019; A. M. Beloborodov 2020), propagation effects would be less severe. In this model, the FRB is produced when an ultra-relativistic flare, generated by a magnetar BNS remnant or a blitzar event, interacts with the mildly relativistic upstream shocked medium.

This scenario, however, faces a significant challenge of its own: in the early phase of ejecta evolution (∼days post-merger), the propagation medium must be baryon-free or "clean" to allow the ultra-relativistic flare to interact with the sub-relativistic shocked medium in far-field models. This condition is very difficult to meet, especially if GW190425 is a highly off-axis event(D. Radice et al. 2016; C. Dean et al. 2021).

Additionally, in the case of FRB 20190425A, there is another challenge that the far-field models face. Baseband data for FRB 20190425A, with a temporal and frequency resolution of 2.56 μs and 0.39 MHz respectively, reveal multiple sub-bursts at timescales $\lesssim 10\,\mu$s (see Figure 1 of J. T. Faber et al. 2024), which are challenging to produce in far-field FRB models (P. Beniamini & P. Kumar 2020; P. Kumar & W. Lu 2020; W. Lu et al. 2022), even when considering nonlinear propagation effects in the relativistic winds of magnetars (E. Sobacchi et al. 2023).

Therefore, we argue that FRB 20190425A is unlikely to have been produced via a far-field mechanism, and its use to explain the GW-FRB association is not favored. However, further investigation is needed to assess the feasibility of far-field models in general for detecting FRBs from BNS merger remnants at short post-merger timescales (∼days).

4.3. Implication for Future FRB-GW Associations

This study underscores that any potential association between FRBs and BNS merger remnants, as discussed in A. Moroianu et al. (2023), must satisfy stringent constraints beyond chance association. A critical constraint is the detectability of FRBs at ∼1 GHz, which depends on the time required for the ejecta to become optically thin, as detailed in Section 3. For an ejecta mass as low as $10^{-2}\,M_{\odot}$, this process could take several months, and the long-term stability of SMNS remnants over this period remains speculative (N. Sarin et al. 2020; P. Beniamini & W. Lu 2021; O. S. Salafia et al. 2022). While it is conceivable that stable neutron star remnants could be the dominant contributors to FRBs from BNS mergers, only a small fraction of BNS mergers are expected to result in such remnants ($\lesssim$1%; P. Beniamini & W. Lu 2021). Given a mean neutron star merger rate of $105\,\mathrm{Gpc^{-3}\,yr^{-1}}$ (R. Abbott et al. 2023) and a typical magnetic activity timescale of 20 yr (A. M. Beloborodov & X. Li 2016; B. Margalit et al. 2019), the local Universe comoving number density of such remnants is estimated to be $\lesssim 21\,\mathrm{Gpc^{-3}\,yr^{-1}}$. Considering the observed local Universe FRB comoving number density ($\gtrsim 10^5\,\mathrm{Gpc^{-3}}$; M. Bhardwaj et al. 2021b), this suggests that less than 1% of FRB sources could be produced by BNS merger remnants.

One potential way to mitigate the challenges posed by propagation effects is for the FRB to travel along the direction of the relativistic jet, as discussed in Section 4.1. This scenario would limit the association to BNS mergers that also produce short GRBs (or sGRBs in short). However, it remains uncertain whether the low-density cavity created by the jet would persist for the necessary duration, ranging from hours to days (R. Ciolfi & J. V. Kalinani 2020; H. Hamidani & K. Ioka 2021). N. Sarin et al. (2022a) estimated that only about 2% of BNS mergers would produce an observable sGRB, which is insufficient to account for the observed volumetric rate of local Universe FRBs. This shortfall is further exacerbated by the fact that only 45%–90% of BNS remnants are expected to form supermassive or stable NSs (P. Beniamini & W. Lu 2021). Therefore, the association between FRBs and postmerger BNS remnants would be exceedingly rare, with only a tiny fraction of FRBs (∼1 in 10,000–100,000 nonrepeating FRBs) meeting the necessary conditions.

5. Conclusion

In this study, we establish essential criteria, based on astrophysical and GW constraints, that must be satisfied for any credible association between FRBs and BNS mergers. These criteria serve as prerequisites for assessing the likelihood of coincidental occurrences of these two events. To demonstrate their utility, we use the proposed association between the GW event GW190425 and FRB 20190425A, as put forth by

A. Moroianu et al. (2023) and F. H. Panther et al. (2022), as a test case. We first use the parameter estimation results using the I. Magaña Hernandez et al. (2024) formalism with the sky location of UGC 10667 as the host galaxy for the FRB 20190425A counterpart. The parameter estimation results yield a stringent constraint on the inclination angle. In order for the association to be valid within the blitzar model, the GW event needs to be on axis. However, our findings indicate that the probability of the viewing angle $p(\theta_v > 30^\circ) \approx 99.99\%$ for both high-spin and low-spin prior scenarios. Furthermore, our analysis demonstrates that in order for the FRB 20190425A to be observed at 400 MHz without significant attenuation, an exceedingly low ejecta mass ($\lesssim 10^{-14} M_\odot$) is required. This value is orders of magnitude smaller than what is typically anticipated based on simulations and observations of BNS mergers. Additionally, we note that in order for the association to make sense, one would require an exotic EOS, as suggested by B. Zhang (2023). We, therefore, argue that GW190425 most likely promptly collapsed into a black hole, a possibility that was also considered by B. P. Abbott et al. (2019). Therefore, we conclude that GW190425 and FRB 20190425A are not related.

Finally, our analysis constrained the volumetric rate of BNS mergers and the birth rate of stable neutron star remnants $\lesssim 21\ \mathrm{Gpc^{-3}\ yr^{-1}}$ that can produce FRBs, which is insufficient to explain the high volumetric rate of FRBs. Hence, we conclude that BNS merger remnants cannot account for the formation of >1% of FRB sources. Consequently, they should not be invoked to characterize the overall population of FRB host galaxies.

In conclusion, we emphasize the need for caution in associating GW and FRB events in future studies. Relying on the probability of chance associations can be insufficient to establish potential associations conclusively. This cautionary approach is particularly crucial due to the significant disparity in the local volumetric rates between BNS events, which are approximately 4 orders of magnitude lower, and FRBs at their fiducial energy of approximately 10^{39} erg. Therefore, it is important to take into account the astrophysical constraints highlighted in this study when considering such associations.

Acknowledgments

The authors would like to thank Bing Zhang, David Radice, Kendall Ackley, and Pawan Kumar for their useful comments and feedback. M.B. is a McWilliams postdoctoral fellow and an International Astronomical Union Gruber fellow. I.M.H. is supported by NSF Award No. PHY-1912649 and PHY-2207728. V.D.E is supported by Science and Technology Facilities Council (STFC) grant ST/V001396/1. The authors are grateful for computational resources provided by the Leonard E Parker Center for Gravitation, Cosmology and Astrophysics at the University of Wisconsin–Milwaukee and supported by NSF awards PHY-1912649, as well as computational resources provided by Cardiff University and supported by STFC grant ST/V001337/1 (UK LIGO Operations award). We thank LIGO and Virgo Collaboration for providing the data for this work. This research has made use of data, software, and/or web tools obtained from the Gravitational Wave Open Science Center (https://www.gw-openscience.org/), a service of LIGO Laboratory, the LIGO Scientific Collaboration, and the Virgo Collaboration. LIGO Laboratory and Advanced LIGO are funded by the United States National Science Foundation (NSF) as well as the Science and Technology Facilities Council (STFC) of the United Kingdom, the Max-Planck-Society (MPS), and the State of Niedersachsen/Germany for support of the construction of Advanced LIGO and construction and operation of the GEO600 detector. Additional support for Advanced LIGO was provided by the Australian Research Council. Virgo is funded, through the European Gravitational Observatory (EGO), by the French Centre National de Recherche Scientifique (CNRS), the Italian Istituto Nazionale di Fisica Nucleare (INFN), and the Dutch Nikhef, with contributions by institutions from Belgium, Germany, Greece, Hungary, Ireland, Japan, Monaco, Poland, Portugal, and Spain. This material is based upon work supported by NSF's LIGO Laboratory, which is a major facility fully funded by the National Science Foundation. This article has been assigned LIGO document number LIGO-P2100449.

ORCID iDs

Mohit Bhardwaj https://orcid.org/0000-0002-3615-3514
Antonella Palmese https://orcid.org/0000-0002-6011-0530
Ignacio Magaña Hernandez https://orcid.org/0000-0003-2362-0459
Virginia D'Emilio https://orcid.org/0000-0001-6145-8187
Soichiro Morisaki https://orcid.org/0000-0002-8445-6747

References

Abazajian, K. N., Adelman-McCarthy, J. K., Agueros, M. A., et al. 2009, ApJS, 182, 543
Abbott, B., Abbott, R., Abbott, T., et al. 2020, ApJ, 892, L3
Abbott, B. P., Abbott, R., Abbott, T. D., et al. 2017, ApJL, 850, L39
Abbott, B. P., Abbott, R., Abbott, T. D., et al. 2019, PhRvX, 9, 011001
Abbott, B. P., Abbott, R., Abbott, T. D., et al. 2020a, ApJL, 892, L3
Abbott, B. P., et al. 2020b, ApJL, 892, L3
Abbott, R., Abbott, T. D., Abraham, S., et al. 2021, ApJ, 915, 86
Abbott, R., Abbott, T. D., Acernese, F., et al. 2023, PhRvX, 13, 041039
Abbott, R., Abbott, T. D., Acernese, F., et al. 2024, PhRvD, 109, 022001
Abramowicz, M. A., Bejger, M., & Wielgus, M. 2018, ApJ, 868, 17
Ahumada, R., Allende Prieto, C., Almeida, A., et al. 2020, ApJS, 249, 3
Andersen, B. C., Bandura, K., Bhardwaj, M., et al. 2023, ApJ, 947, 83
Arons, J., & Barnard, J. J. 1986, ApJ, 302, 120
Ashton, G., Hubner, M., Lasky, P. D., et al. 2019, ApJS, 241, 27
Barbieri, C., Salafia, O. S., Colpi, M., Ghirlanda, G., & Perego, A. 2021, A&A, 654, A12
Baylor, A., Smith, R., & Chase, E. 2019, IMRPhenomPv2_NRTidal_GW190425_narrow_Mc v1, Zenodo, doi:10.5281/zenodo.3478659
Beloborodov, A. M. 2020, ApJ, 896, 142
Beloborodov, A. M., & Li, X. 2016, ApJ, 833, 261
Beniamini, P., & Kumar, P. 2020, MNRAS, 498, 651
Beniamini, P., & Lu, W. 2021, ApJ, 920, 109
Bhardwaj, M., Gaensler, B. M., Kaspi, V. M., et al. 2021a, ApJL, 910, L18
Bhardwaj, M., Kirichenko, A. Y., Michilli, D., et al. 2021b, ApJL, 919, L24
Bhardwaj, M., Michilli, D., Kirichenko, A. Y., et al. 2024, ApJ, 971, L51
Biscoveanu, S., Thrane, E., & Vitale, S. 2020, ApJ, 893, 38
Bucciantini, N., Thompson, T. A., Arons, J., Quataert, E., & Del Zanna, L. 2006, MNRAS, 368, 1717
Bühler, R., & Giomi, M. 2016, MNRAS, 462, 2762
Burns, E. 2020, LRR, 23, 4
Caleb, M., & Keane, E. 2021, Univ, 7, 453
CHIME/FRB Collaboration, Amiri, M., Andersen, B. C., et al. 2021, ApJS, 257, 59
CHIME/FRB Collaboration, Amiri, M., Bandura, K., et al. 2019a, Natur, 566, 235
CHIME/FRB Collaboration, Andersen, B. C., Bandura, K., et al. 2019b, ApJL, 885, L24
Ciolfi, R., & Kalinani, J. V. 2020, ApJL, 900, L35
Cordes, J. M., & Chatterjee, S. 2019, ARA&A, 57, 417
Cordes, J. M., & Lazio, T. J. W. 2002, arXiv:astro-ph/0207156
Coughlin, M. W., Ahumada, T., Anand, S., et al. 2019, ApJ, 885, L19
Coughlin, M. W., Dietrich, T., Doctor, Z., et al. 2018, MNRAS, 480, 3871
Darbha, S., & Kasen, D. 2020, ApJ, 897, 150

Dean, C., Fernández, R., & Metzger, B. D. 2021, ApJ, 921, 161
Dessart, L., Ott, C. D., Burrows, A., Rosswog, S., & Livne, E. 2009, ApJ, 690, 1681
Dietrich, T., Bernuzzi, S., & Tichy, W. 2017, PhRvD, 96, 121501
Dietrich, T., Bernuzzi, S., Ujevic, M., & Brügmann, B. 2015, PhRvD, 91, 124041
Dietrich, T., Khan, S., Dudi, R., et al. 2019, PhRvD, 99, 024029
Dudi, R., Adhikari, A., Brügmann, B., et al. 2022, PhRvD, 106, 084039
Essick, R., & Landry, P. 2020, ApJ, 904, 80
Faber, J. T., Michilli, D., Mckinven, R., et al. 2024, ApJ, 974, 274
Falcke, H., & Rezzolla, L. 2014, A&A, 562, A137
Foley, R. J., Coulter, D. A., Kilpatrick, C. D., et al. 2020, MNRAS, 494, 190
Fonseca, E., Andersen, B. C., Bhardwaj, M., et al. 2020, ApJL, 891, L6
Gao, H., Ai, S.-K., Cao, Z.-J., et al. 2020, FrPhy, 15, 24603
Giacomazzo, B., Zrake, J., Duffell, P. C., MacFadyen, A. I., & Perna, R. 2015, ApJ, 809, 39
Gourdji, K., Rowlinson, A., Wijers, R. A. M. J., & Goldstein, A. 2020, MNRAS, 497, 3131
Granot, J., Gill, R., Guetta, D., & De Colle, F. 2018, MNRAS, 481, 1597
Gürlebeck, N. 2015, PhRvL, 114, 151102
Hamidani, H., & Ioka, K. 2021, MNRAS, 500, 627
Han, M.-Z., Tang, S.-P., Hu, Y.-M., et al. 2020, ApJL, 891, L5
Henkel, A., Foucart, F., Raaijmakers, G., & Nissanke, S. 2023, PhRvD, 107, 063028
Hosseinzadeh, G., Cowperthwaite, P. S., Gomez, S., et al. 2019, ApJ, 880, L4
Hotokezaka, K., Kiuchi, K., Kyutoku, K., et al. 2013, PhRvD, 87, 024001
Jin, Z.-P., Li, X., Wang, H., et al. 2018, ApJ, 857, 128
Kasen, D., Metzger, B., Barnes, J., Quataert, E., & Ramirez-Ruiz, E. 2017, Natur, 551, 80
Krüger, C. J., & Foucart, F. 2020, PhRvD, 101, 103002
Kumar, P., & Lu, W. 2020, MNRAS, 494, 1217
Kumar, P., Lu, W., & Bhattacharya, M. 2017, MNRAS, 468, 2726
Kumar, P., Shannon, R. M., Flynn, C., et al. 2021, MNRAS, 500, 2525
Lanman, A. E., Andersen, B. C., Chawla, P., et al. 2022, ApJ, 927, 59
Levinson, A., & Blandford, R. 1995, MNRAS, 274, 717
Li, A., Zhang, B., Zhang, N.-B., et al. 2016, PhRvD, 94, 083010
Lorimer, D. R., Bailes, M., McLaughlin, M. A., Narkevic, D. J., & Crawford, F. 2007, Sci, 318, 777
Lu, W., Beniamini, P., & Kumar, P. 2022, MNRAS, 510, 1867
Lyubarsky, Y. 2008, ApJ, 682, 1443
Macquart, J.-P., Prochaska, J. X., McQuinn, M., et al. 2020, Natur, 581, 391
Magaña Hernandez, I., D'Emilio, V., Morisaki, S., Bhardwaj, M., & Palmese, A. 2024, ApJL, 971, L5
Margalit, B., Berger, E., & Metzger, B. D. 2019, ApJ, 886, 110
Martin, D., Perego, A., Arcones, A., et al. 2015, ApJ, 813, 2
McKinven, R. & CHIME/FRB Collaboration 2022, ATel, 15679, 1
Melrose, D. B. 1972, Ap&SS, 18, 267
Metzger, B. D. 2019, LRR, 23, 1
Metzger, B. D., Beniamini, P., & Giannios, D. 2018, ApJ, 857, 95
Metzger, B. D., Margalit, B., & Sironi, L. 2019, MNRAS, 485, 4091
Mingarelli, C. M. F., Levin, J., & Lazio, T. J. W. 2015, ApJL, 814, L20
Moroianu, A., Wen, L., James, C. W., et al. 2023, NatAs, 7, 579
Niu, C. H., Aggarwal, K., Li, D., et al. 2022, Natur, 606, 873
Palenzuela, C., Aguilera-Miret, R., Carrasco, F., et al. 2022, PhRvD, 106, 023013
Panther, F. H., Anderson, G. E., Bhandari, S., et al. 2022, MNRAS, 519, 2235
Perego, A., Radice, D., & Bernuzzi, S. 2017, ApJL, 850, L37
Perego, A., Rosswog, S., Cabezón, R. M., et al. 2014, MNRAS, 443, 3134
Petroff, E., Hessels, J. W. T., & Lorimer, D. R. 2022, A&ARv, 30, 2
Planck Collaboration, Ade, P. A. R., Aghanim, N., et al. 2015, A&A, 594, A13
Pozanenko, A. S., Minaev, P. Y., Grebenev, S. A., & Chelovekov, I. V. 2020, AstL, 45, 710
Radice, D., Galeazzi, F., Lippuner, J., et al. 2016, MNRAS, 460, 3255
Radice, D., Perego, A., Hotokezaka, K., et al. 2018, ApJ, 869, 130
Radice, D., Ricigliano, G., Bhattacharya, M., et al. 2024, MNRAS, 528, 5836
Ravi, V., & Loeb, A. 2019, ApJ, 874, 72
Razin, V. 1960, RaF, 3, 584
Romero-Shaw, I. M., Talbot, C., Biscoveanu, S., et al. 2020, MNRAS, 499, 3295
Ruiz, M., Lang, R. N., Paschalidis, V., & Shapiro, S. L. 2016, ApJL, 824, L6
Salafia, O. S., Colombo, A., Gabrielli, F., & Mandel, I. 2022, A&A, 666, A174
Sarin, N., Lasky, P. D., & Ashton, G. 2020, PhRvD, 101, 063021
Sarin, N., Lasky, P. D., Vivanco, F. H., et al. 2022a, PhRvD, 105, 083004
Sarin, N., Omand, C. M. B., Margalit, B., & Jones, D. I. 2022b, MNRAS, 516, 4949
Schutz, B. F. 2011, CQGra, 28, 125023
Shin, K., Masui, K. W., Bhardwaj, M., et al. 2023, ApJ, 944, 105
Smartt, S., Nicholl, M., Srivastav, S., et al. 2024, MNRAS, 528, 2299
Smith, R., Field, S. E., Blackburn, K., et al. 2016, PhRvD, 94, 044031
Sneppen, A., Watson, D., Bauswein, A., et al. 2023, Natur, 614, 436
Sobacchi, E., Lyubarsky, Y., Beloborodov, A. M., Sironi, L., & Iwamoto, M. 2023, ApJL, 943, L21
Speagle, J. S. 2020, MNRAS, 493, 3132
Spitler, L. G., Scholz, P., Hessels, J. W. T., et al. 2016, Natur, 531, 202
The LIGO Scientific Collaboration, the Virgo Collaboration, the KAGRA Collaboration, et al. 2023, ApJ, 955, 155
Thompson, T. A., Chang, P., & Quataert, E. 2004, ApJ, 611, 380
Totani, T. 2013, PASJ, 65, L12
Wang, F. Y., Wang, Y. Y., Yang, Y.-P., et al. 2020, ApJ, 891, 72
Wang, J.-S., Yang, Y.-P., Wu, X.-F., Dai, Z.-G., & Wang, F.-Y. 2016, ApJL, 822, L7
Wilson, D. B. 1982, MNRAS, 200, 881
Wu, G.-L., Yu, Y.-W., & Li, S.-Z. 2022, Univ, 8, 633
Yamasaki, S., & Totani, T. 2020, ApJ, 888, 105
Yamasaki, S., Totani, T., & Kiuchi, K. 2018, PASJ, 70, 39
Yao, J. M., Manchester, R. N., & Wang, N. 2017, ApJ, 835, 29
Yaron, O., Ofek, E., Gal-Yam, A., & Sass, A. 2020, TNSAN, 70, 1
Zhang, B. 2014, ApJL, 780, L21
Zhang, B. 2016, ApJL, 827, L31
Zhang, B. 2023, RvMP, 95, 035005